

Necklaces of PT-symmetric dimers

D. J. NODAL STEVENS,¹ BENJAMÍN JARAMILLO ÁVILA,² AND B. M. RODRÍGUEZ-LARA^{1,3,*} 

¹Tecnologico de Monterrey, Escuela de Ingeniería y Ciencias, Ave. Eugenio Garza Sada 2501, Monterrey, N.L. 64849, Mexico

²CONACYT–Instituto Nacional de Astrofísica, Óptica y Electrónica, Calle Luis Enrique Erro No. 1, Sta. Ma. Tonantzintla, Pue. CP 72840, Mexico

³Instituto Nacional de Astrofísica, Óptica y Electrónica, Calle Luis Enrique Erro No. 1, Sta. Ma. Tonantzintla, Pue. CP 72840, Mexico

*Corresponding author: bmlara@itesm.mx

Received 5 September 2017; revised 25 January 2018; accepted 9 February 2018; posted 9 February 2018 (Doc. ID 306303); published 4 April 2018

We study light propagation through cyclic arrays, composed by copies of a given PT-symmetric dimer, using a group theoretical approach and finite element modeling. The theoretical mode-coupling analysis suggests the use of these devices as output port replicators where the dynamics is controlled by the impinging light field. This is confirmed in good agreement with finite element propagation in an experimentally feasible necklace of passive PT-symmetric dimers constructed from lossy and lossless waveguides. © 2018 Chinese Laser Press

OCIS codes: (230.7370) Waveguides; (130.2790) Guided waves; (140.4480) Optical amplifiers; (000.1600) Classical and quantum physics.

<https://doi.org/10.1364/PRJ.6.000A31>

1. INTRODUCTION

Photonic device designers have been toying with the idea of using gain and loss in linear [1] and nonlinear [2] optical systems in order to produce unidirectional couplers or low intensity switches, in that order, for a long time. The advent of parity time (PT) symmetry in quantum mechanics [3,4], the idea that non-Hermitian Hamiltonians invariant under space–time reflection might possess a real spectrum, brought a new structure to these approaches. Two ideas made use of this quantum mechanical tool to describe a planar slab waveguide [5] and coupled optical structures with symmetric gain and losses [6]. The latter became seminal for the field of PT-symmetric photonics and has inspired a plethora of optical proposals [7,8].

The quintessential PT-symmetric optical device is the balanced gain and loss dimer that has been experimentally realized in diverse optical platforms [9–13]. It can be understood as a finite, nonunitary realization of the Lorentz group [14] allowing for three types of propagation dynamics: periodic field amplitude oscillation with amplification, as well as linear and exponential field amplitude amplification. The first case corresponds to the PT-symmetric regime, where eigenvalues are real. The second case is the Kato exceptional point, where the eigenvalues are degenerate and equal to zero. The third case displays PT-symmetry breaking, where the two eigenvalues are purely imaginary and the complex conjugates of each other. It is also known that any optical realization of the Lorentz group in the broken PT-symmetric regime shows asymptotic behavior, for renormalized intensities, that depends only on the interplay of gain and coupling parameters for both linear [14] and nonlinear systems [7].

We are interested in a natural extension of the nonlinear PT-symmetric dimer: its periodic repetition over a circular loop. Light propagation through these so-called necklaces where individual waveguides are homogeneously spaced has been shown to (dis)allow a PT-symmetric regime for (even) odd repetition of the dimer [15]. The nonlinear four-waveguide array is known to produce an asymmetric distribution of optical power [16], to possess continuous families of nonlinear modes [17], and it is not PT symmetric in the usual matrix sense [18]. The absence of exceptional points, for homogeneous arrays of dimension four, was discussed using linear arrays of four sub-wavelength waveguides [19], while the possibility to restore PT symmetry through mechanical action has also been shown [20].

Here, we will construct a slightly more general system where the standard PT-symmetric dimer is repeated for N times over a circular loop, with the addition of constant intra- and inter-dimer coupling lengths that are different from each other, as shown in Fig. 1(a). Such a model can be realized in laser inscribed arrays of waveguides, circular multicore fibers, toroidal cavities, or electronic systems. In the following sections, we introduce the model and show that it can be composed using the cyclic and Lorentz groups. We will use a group theory approach to further the idea that discrete symmetries in photonics are a powerful design tool [21]. Then, we diagonalize our coupled mode model in the cyclic group basis to show that its dynamics is consistent with those of uncoupled effective dimers with variable couplings. We discuss the eigenvalues of these effective dimers and show that homogeneously distributed necklaces with even numbers of copies always have at least a pair of imaginary eigenvalues and PT symmetry can be restored by making

the intra- and inter-dimer couplings different. Then, we show that the underlying cyclic symmetry suggests the use of these photonic devices as output replicators, where input light is used to select the effective dynamics to replicate in the outputs. We provide finite element simulations to justify our analytic approach using data from experimental work on waveguide laser inscription in silicon. We close our article with a brief summary and conclusion.

2. LINEAR MODEL AND ITS UNDERLYING SYMMETRY

The coupled mode formalism for a tightly bound necklace formed by N identical PT-symmetric dimers yields the following set of differential equations:

$$\begin{aligned}
 -i\partial_z \mathcal{E}_0(z) &= i\gamma \mathcal{E}_0(z) + g_d e^{-i\phi_d} \mathcal{E}_1(z) + g_N e^{i\phi_N} \mathcal{E}_{2N-1}(z), \\
 -i\partial_z \mathcal{E}_1(z) &= -i\gamma \mathcal{E}_1(z) + g_d e^{i\phi_d} \mathcal{E}_0(z) + g_N e^{-i\phi_N} \mathcal{E}_2(z), \\
 &\vdots \\
 -i\partial_z \mathcal{E}_{2j}(z) &= i\gamma \mathcal{E}_{2j}(z) + g_d e^{-i\phi_d} \mathcal{E}_{2j+1}(z) + g_N e^{i\phi_N} \mathcal{E}_{2j-1}(z), \\
 -i\partial_z \mathcal{E}_{2j+1}(z) &= -i\gamma \mathcal{E}_{2j+1}(z) + g_d e^{i\phi_d} \mathcal{E}_{2j}(z) + g_N e^{-i\phi_N} \mathcal{E}_{2j+2}(z), \\
 &\vdots \\
 -i\partial_z \mathcal{E}_{2N-2}(z) &= i\gamma \mathcal{E}_{2N-2}(z) + g_d e^{-i\phi_d} \mathcal{E}_{2N-1}(z) + g_N e^{i\phi_N} \mathcal{E}_{2N-3}(z), \\
 -i\partial_z \mathcal{E}_{2N-1}(z) &= -i\gamma \mathcal{E}_{2N-1}(z) + g_d e^{i\phi_d} \mathcal{E}_{2N-2}(z) + g_N e^{-i\phi_N} \mathcal{E}_0(z),
 \end{aligned} \tag{1}$$

for the field mode amplitude at each fiber, described by the complex-valued functions $\mathcal{E}_n(z)$ with $n = 0, \dots, 2N - 1$. Our optical system generalizes a previous homogeneously coupled periodic array studied in Ref. [15] by allowing different intra(inter)-dimer couplings, $g_d e^{-i\phi_d}$ ($g_N e^{-i\phi_N}$), where the coupling strength, g_d (g_N), and coupling phases, ϕ_d (ϕ_N), are real. The coupling phases can be induced by mechanical twisting in optical fibers or capacitive coupling in electronic systems. Finally, gains and losses in the fibers are quantified by the real

parameter γ . Our periodic array of coupled waveguides is sketched in Fig. 1(a) for the general necklace; we also show sketches for specific realization like the standard PT-symmetric dimer, Fig. 1(b), the PT-symmetric plaquette, Fig. 1(c), and a necklace composed by three dimers, Fig. 1(d). Later, we will focus on the last two of these realizations.

The coupled mode equations in Eq. (1) can be written in a more compact way using Dirac notation,

$$-i\partial_z |\mathcal{E}(z)\rangle = \hat{H} |\mathcal{E}(z)\rangle, \tag{2}$$

where the ket $|\mathcal{E}(z)\rangle$ is a simple vector collecting the $2N$ field mode amplitudes in our model,

$$|\mathcal{E}(z)\rangle = \begin{pmatrix} \mathcal{E}_0(z) \\ \mathcal{E}_1(z) \\ \mathcal{E}_2(z) \\ \mathcal{E}_3(z) \\ \vdots \\ \mathcal{E}_{2N-2}(z) \\ \mathcal{E}_{2N-1}(z) \end{pmatrix} \left\{ \begin{array}{l} (j=0) \text{ - th dimer} \\ (j=1) \text{ - th dimer} \\ \vdots \\ (j=N-1) \text{ - th dimer} \end{array} \right. \begin{array}{l} k=0 \\ k=1 \\ k=0 \\ k=1 \\ \vdots \\ k=0 \\ k=1 \end{array} . \tag{3}$$

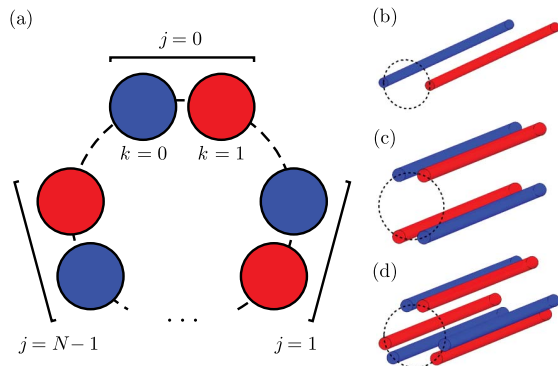


Fig. 1. Sketch for necklaces formed by the repetition of identical PT-symmetric dimers. (a) Necklace where intradimer couplings are larger than interdimer couplings, $g_d > g_N$, and repetition factor N . (b) Standard PT-symmetric dimer, $N = 1$; (c) PT-symmetric plaquette, $N = 2$; and (d) necklace with repetition factor $N = 3$.

The mode-coupling matrix is represented by the operator \hat{H} , a block-tridiagonal $2N \times 2N$ matrix which can be written using $N \times N$ blocks of 2×2 matrices,

$$\hat{H} = \begin{pmatrix} \hat{H}_d & \hat{H}_- & \hat{\mathbb{O}}_2 & \dots & \hat{\mathbb{O}} & \hat{H}_+ \\ \hat{H}_+ & \hat{H}_d & \hat{H}_- & \dots & \hat{\mathbb{O}} & \hat{\mathbb{O}} \\ \hat{\mathbb{O}} & \hat{H}_+ & \hat{H}_d & \ddots & \hat{\mathbb{O}} & \hat{\mathbb{O}} \\ \vdots & \vdots & \ddots & \ddots & \ddots & \vdots \\ \hat{\mathbb{O}} & \hat{\mathbb{O}} & \hat{\mathbb{O}} & \ddots & \hat{H}_d & \hat{H}_- \\ \hat{H}_- & \hat{\mathbb{O}} & \hat{\mathbb{O}} & \dots & \hat{H}_+ & \hat{H}_d \end{pmatrix}, \tag{4}$$

where the symbol $\hat{\mathbb{O}}$ stands for the 2×2 zero matrix, and the auxiliary block matrices,

$$\begin{aligned}\hat{H}_d &= \begin{pmatrix} i\gamma & g_d e^{-i\phi_d} \\ g_d e^{i\phi_d} & -i\gamma \end{pmatrix}, & \hat{H}_+ &= \begin{pmatrix} 0 & g_N e^{i\phi_N} \\ 0 & 0 \end{pmatrix}, \\ \hat{H}_- &= \begin{pmatrix} 0 & 0 \\ g_N e^{-i\phi_N} & 0 \end{pmatrix},\end{aligned}\quad (5)$$

describe the repeating PT-symmetric dimer, \hat{H}_d , and the interdimer couplings, \hat{H}_\pm . These matrices can be rewritten in operator notation,

$$\hat{H}_d = \gamma i\hat{\sigma}_z + g_d e^{-i\phi_d} \hat{\sigma}_+ + g_d e^{i\phi_d} \hat{\sigma}_-, \quad \hat{H}_\pm = g_N e^{\pm i\phi_N}, \quad (6)$$

where the operators $\{\hat{\sigma}_z, \hat{\sigma}_\pm\}$ are related to the SO(2,1) Lie group [7,14], the Lorentz group in (2 + 1) dimensions, and relate to Pauli matrices,

$$\hat{\sigma}_z = \begin{pmatrix} 1 & 0 \\ 0 & -1 \end{pmatrix}, \quad \hat{\sigma}_+ = \begin{pmatrix} 0 & 1 \\ 0 & 0 \end{pmatrix}, \quad \hat{\sigma}_- = \begin{pmatrix} 0 & 0 \\ 1 & 0 \end{pmatrix}. \quad (7)$$

In addition, our necklace is invariant to rotations of $2\pi/N$ rad around its center; in other words, it has an underlying \mathbb{Z}_N symmetry provided by the cyclic group of dimension N . The cyclic group is generated by the N powers of the so-called shift operator, \hat{C}_N^j , with $j = 1, 2, \dots, N$. These shift operators are $N \times N$ matrices in the representation at hand,

$$\begin{aligned}\hat{C}_N &= \begin{pmatrix} 0 & 0 & 0 & \dots & 0 & 1 \\ 1 & 0 & 0 & \dots & 0 & 0 \\ 0 & 1 & 0 & \ddots & 0 & 0 \\ \vdots & \vdots & \ddots & \ddots & \ddots & \vdots \\ 0 & 0 & 0 & \ddots & 0 & 0 \\ 0 & 0 & 0 & \dots & 1 & 0 \end{pmatrix}, \\ \hat{C}_N^\dagger &= \begin{pmatrix} 0 & 1 & 0 & \dots & 0 & 0 \\ 0 & 0 & 1 & \dots & 0 & 0 \\ 0 & 0 & 0 & \ddots & 0 & 0 \\ \vdots & \vdots & \ddots & \ddots & \ddots & \vdots \\ 0 & 0 & 0 & \ddots & 0 & 1 \\ 1 & 0 & 0 & \dots & 0 & 0 \end{pmatrix}.\end{aligned}\quad (8)$$

Note that the adjoint of the shift operator is given by the relation $\hat{C}_N^\dagger = \hat{C}_N^{N-1}$, and the corresponding unit matrix is simply $\hat{C}_N^N = \hat{\mathbb{1}}_N$. We can use the fact that our PT-symmetric necklace possesses an underlying $\mathbb{Z}_N \otimes \text{SO}(2, 1)$ symmetry to rewrite its mode-coupling matrix,

$$\hat{H} = \hat{\mathbb{1}}_N \otimes \hat{H}_d + \hat{C}_N \otimes \hat{H}_+ + \hat{C}_N^\dagger \otimes \hat{H}_-, \quad (9)$$

using the Kronecker (outer) product of operators (matrices) belonging to the two symmetries described before.

This underlying symmetry will also manifest in the field mode amplitude vector, Eq. (3), and we use this fact to rewrite it in a compact way,

$$|\mathcal{E}(z)\rangle = \sum_{j=0}^{N-1} \sum_{k=0}^1 \mathcal{E}_{2j+k}(z) |j\rangle_N \otimes |k\rangle_2, \quad (10)$$

using the collection of N -dimensional orthogonal vectors $|j\rangle_N = (0, \dots, 0, 1, 0, \dots, 0)^T$, where only the $(j + 1)$ -th component has a value of one and the rest are null, and the two-dimensional orthogonal vectors $|0\rangle_2 = (1, 0)^T$ and $|1\rangle_2 = (0, 1)^T$. The complex functions $\mathcal{E}_{2j+k}(z)$, with $j = 0, 1, \dots, N - 1$ and $k = 0, 1$, are the components of the $2N$ -dimensional vector $|\mathcal{E}(z)\rangle$ in Eq. (3).

3. PT SYMMETRY AND PROPAGATION IN THE LINEAR DIMER

We can take advantage of the underlying symmetries of our necklace. It is well known that the Fourier matrix [22],

$$\hat{F}_N = \frac{1}{\sqrt{N}} \sum_{j,k=0}^{N-1} e^{i\frac{2\pi}{N}jk} |j\rangle \langle k|, \quad (11)$$

diagonalizes the cyclic group shift operator into the so-called clock matrix,

$$\hat{\Lambda}_N = \hat{F}_N \hat{C}_N \hat{F}_N^\dagger = \sum_{j=0}^{N-1} e^{i\frac{2\pi}{N}j} |j\rangle \langle j|. \quad (12)$$

Note that we have obviated the dimension subindex N in the outer product, $|j\rangle \langle k| \equiv |j\rangle_N \otimes_N \langle k|$, of column, $|j\rangle_N$, and row, $\langle k|_N$, vectors.

Thus, we can suggest a change of vector basis provided by the Fourier matrix basis,

$$|\mathcal{E}(z)\rangle = (\hat{F}_N \otimes \hat{\mathbb{1}}_2)^\dagger |\mathcal{A}(z)\rangle, \quad (13)$$

and recover effective propagation dynamics,

$$-i\partial_z |\mathcal{A}(z)\rangle = \hat{H}_D |\mathcal{A}(z)\rangle \quad (14)$$

described by a block-diagonal mode-coupling matrix,

$$\hat{H}_D = \sum_{j=0}^{N-1} |j\rangle \langle j| \otimes \hat{H}_j, \quad (15)$$

where each diagonal block describes a PT-symmetric dimer whose effective coupling depends on its position in the diagonal,

$$\hat{H}_j = i\gamma \hat{\sigma}_z + [\Gamma_j \hat{\sigma}_+ + \Gamma_j^* \hat{\sigma}_-], \quad (16)$$

with the new effective complex coupling given by the following expression,

$$\Gamma_j = g_d e^{-i\phi_d} + g_N e^{i\phi_N} e^{i\frac{2\pi}{N}j}. \quad (17)$$

Here, it is straightforward to calculate the eigenvalues of these matrices,

$$\begin{aligned}\lambda_{\pm j} &= \pm \sqrt{|\Gamma_j|^2 - \gamma^2}, \\ &= \pm \sqrt{g_d^2 + g_N^2 + 2g_d g_N \cos\left(\phi_d + \phi_N + \frac{2\pi}{N}j\right) - \gamma^2},\end{aligned}\quad (18)$$

and realize that different intra- and inter-dimer complex couplings can restore the PT-symmetric phase to systems lacking it. For example, homogeneously coupled arrays, $g_d = g_N = g$

with $\phi_d = \phi_N = 0$, with even repetition number, $N = 2n$ with $n = 1, 2, 3, \dots$, lack a PT-symmetric phase [15]. This phase can be restored using inhomogeneous intra- and interdimer couplings, $g_d \neq g_N$, in an adequate way. Note that inhomogeneous couplings raise soliton stability thresholds in infinite nonlinear PT-symmetric dimer ladders [23], suggesting a possible stabilizing role for such couplings.

In homogeneously coupled arrays, the block \hat{H}_0 is the standard PT-symmetric dimer with Kato exceptional point $\gamma = 2g$. Each block will have its own exceptional point at the following values of the gain to coupling ratio,

$$\frac{\gamma}{2g} = \cos \frac{2\pi}{N} j, j = 0, 1, 2, \dots \left\lfloor \frac{N}{2} \right\rfloor \left(\left\lfloor \frac{N}{2} \right\rfloor - 1 \right), \quad (19)$$

for even (odd) dimensions of the cyclic group component, N ; the floor operation $\lfloor \cdot \rfloor$ provides the lowest integer that is less than or equal to its argument. Then, we can realize that arrays where the dimer is repeated for an even number of times always have a pair of complex eigenvalues, $\lambda_{\pm N/2} = \pm i\gamma$, that correspond to the block $\hat{H}_{N/2}$. These arrays do not have a PT-symmetric phase. We can also see that there are pairs of diagonal blocks that are the transpose of each other, $\hat{H}_k = \hat{H}_{N-k}^T$ with $k = 1, 2, \dots, \lfloor N/2 \rfloor - 1$ ($\lfloor N/2 \rfloor$) for even (odd) dimension N . This immediately points to the fact that there will be $\lfloor N/2 \rfloor - 1$ ($\lfloor N/2 \rfloor$) two-fold degenerate eigenvalues in the arrays when the repetition number N is even (odd). Furthermore, the number of imaginary eigenvalues will increase each time the gain to coupling ratio reaches the value for the exceptional point of each block. Figure 2 shows the real to complex eigenvalue transition for necklaces composed of four, Fig. 2(a), and six, Fig. 2(b), waveguides. The simple change of interdimer coupling is enough to induce a PT-symmetric phase in arrays with even repetition number, but the behavior of the degeneracies and the systemic increase in the number of complex eigenvalues remains universal. Figures 2(c) and 2(d) show the eigenvalues of an array where the intradimer couplings are half the value of the

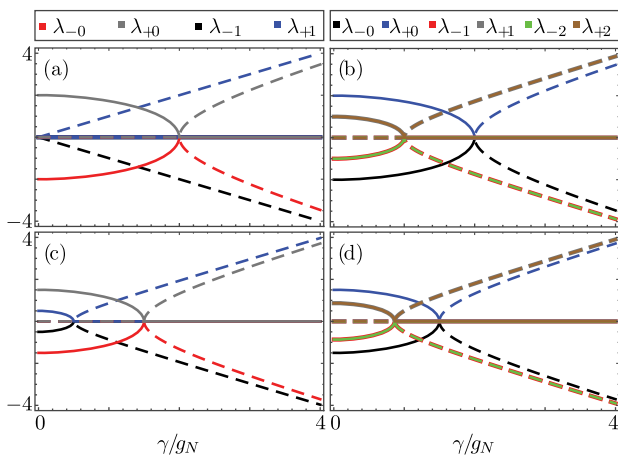


Fig. 2. Real (solid lines) and imaginary (dashed lines) parts of eigenvalues as a function of the gain to interdimer coupling ratio, γ/g_N , for arrays of coupled PT-symmetric dimers with homogeneous intra- and inter-dimer couplings, $g_d = g_N$ with repetition factor (a) $N = 2$ and (b) $N = 3$, and for inhomogeneous couplings, $g_d = g_N/2$, with repetition factor (c) $N = 2$ and (d) $N = 3$.

interdimer couplings, $g_d = g_N/2$. Control of couplings phases, ϕ_d and ϕ_N , introduces another physical parameter to manipulate the type of eigenvalues in the system.

The block diagonal, \hat{H}_D , form of our necklace allows us to construct a propagator for the field mode amplitudes. In the original frame, the propagation of the complex field amplitudes vector,

$$|\mathcal{E}(z)\rangle = \hat{U}(z)|\mathcal{E}(0)\rangle, \quad (20)$$

is provided by the propagator matrix,

$$\hat{U}(z) = \sum_{j=0}^{N-1} \hat{F}_N^\dagger |j\rangle \langle j| \hat{F}_N \otimes e^{i\hat{H}_j z}, \quad (21)$$

in terms of the propagation matrix of each individual effective dimer [24],

$$e^{i\hat{H}_j z} = \hat{\mathbb{1}}_2 \cos \Omega_j z + iz \hat{H}_j \text{sinc } \Omega_j z, \quad (22)$$

where we have used the cardinal sine function, $\text{sinc } x = (\sin x)/x$, and the propagation constant,

$$\Omega_j = \sqrt{|\Gamma_j|^2 - \gamma^2}, \quad (23)$$

is just the positive eigenvalue of the mode-coupling matrix. It takes real values in the PT-symmetric regime, providing a non-unitary oscillator,

$$e^{i\hat{H}_j z} = \hat{\mathbb{1}}_2 \cos \Omega_j z + \frac{i}{\Omega_j} \hat{H}_j \sin \Omega_j z, \quad \Omega_j \in \mathbb{R}. \quad (24)$$

At Kato's exceptional point it has zero value and provides linear amplification and attenuation of the field amplitudes [25],

$$e^{i\hat{H}_j z} = \hat{\mathbb{1}}_2 + iz \hat{H}_j, \quad \Omega_j = 0. \quad (25)$$

Finally, it takes purely imaginary values in the broken symmetry regime, providing exponential amplification and attenuation of the field amplitudes,

$$e^{i\hat{H}_j z} = \hat{\mathbb{1}}_2 \cosh |\Omega_j| z + \frac{i}{|\Omega_j|} \hat{H}_j \sinh |\Omega_j| z, \quad \Omega_j \in \mathbb{C}. \quad (26)$$

4. DIMER OUTPUT REPLICATION

Cyclic symmetry has a curious signature. Whenever such a symmetry is present, we can address specific block diagonal elements and produce N copies of its dynamics. In our necklace, this is produced by the following initial field mode amplitude vector,

$$\begin{aligned} |\mathcal{E}(0)\rangle &= \hat{F}_N^\dagger |j\rangle \otimes |\psi(0)\rangle, \\ &= \frac{1}{\sqrt{N}} \sum_{a=0}^{N-1} e^{i\frac{2\pi}{N} a j} |a\rangle \otimes |\psi(0)\rangle; \end{aligned} \quad (27)$$

that is, the outer product between a vector whose components are all the N th roots of the unit, and some initial states for the effective j th block diagonal dimer we want to address. Such an initial impinging field produces replication, up to a phase, of the dynamics provided by the j th effective dimer,

$$|\mathcal{E}(z)\rangle = \frac{1}{\sqrt{N}} \sum_{p=0}^{N-1} e^{i\frac{2\pi p}{N}} |p\rangle \otimes e^{i\hat{H}_j z} |\psi(0)\rangle, \quad (28)$$

in each and every one of the dimers in the necklace. A simple permutation of input phases allows switching the necklace output, provided that one does not switch to the degenerate pair of the effective dimers, $\hat{H}_j = \hat{H}_{N-j}^T$.

It is well known that outside the PT-symmetric regime, the renormalized power at the k th waveguide within the j th dimer,

$$P_{j,k}(z) = \frac{|\langle k|e^{i\hat{H}_j z}|\psi(0)\rangle|^2}{\sum_{k=0}^1 |\langle k|e^{i\hat{H}_j z}|\psi(0)\rangle|^2}, \quad (29)$$

will show an asymptotic behavior [7,14],

$$\lim_{z \rightarrow \infty} P_{j,0}(z) = \frac{\gamma - |\Omega_j|}{2\gamma}, \quad \lim_{z \rightarrow \infty} P_{j,1}(z) = \frac{\gamma + |\Omega_j|}{2\gamma}, \quad (30)$$

dictated by the parameters of the corresponding effective dimer \hat{H}_j . Thus, we can engineer photonic devices where all the dimers present the same output, and switch from oscillatory to asymptotic behaviors by permutation of the input field phases.

This type of dimer output port replication could be observed in any physically plausible realization of our necklace. For example, let us consider the case of laser inscribed waveguides in silicon, c:Si, for telecommunication wavelength, $\lambda = 1550$ nm. Current techniques allow for control of refractive index properties, $\Delta n = n_{\text{core}} - n_{\text{bulk}} \in [1, 6] \times 10^{-3}$, as well as losses, [0.1,3] dB/cm, with waveguide length of about a centimeter [26,27]. We use the commercial finite element software COMSOL to simulate necklaces of two and three identical copies of a passive PT-symmetric dimer. We use an automatically generated free triangular mesh with size element in the range $[\lambda/2, \lambda]$ in the plane perpendicular to the propagation direction, and a fixed mesh with element size of 15 μm in the propagation direction. The latter is of utmost importance when relative phases are involved. The necklaces are composed by four and six waveguides, each one with a radius $r = 2.232$ μm , in the configurations shown in Fig. 3(a) [Fig. 5(a)] for two (three) dimers. Each dimer is realized by a lossy and a lossless waveguide. The lossy waveguide has complex refractive index $n_{0,0} = n_{1,0} = n_{2,0} = 3.465 + i(2.122 \times 10^{-4})$, and the

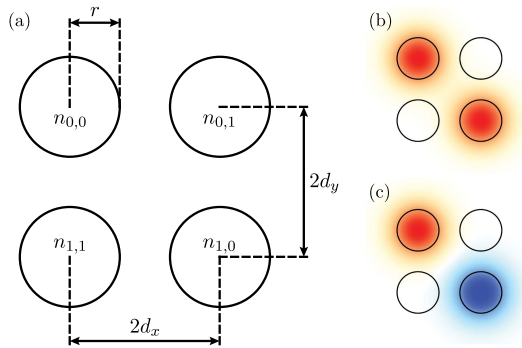


Fig. 3. (a) Waveguide geometry used in the finite element simulation and electric field input for replication of the (b) first and (c) second effective dimers. In (b) and (c), red corresponds to an in-phase beam and blue corresponds to a π -dephased beam.

lossless waveguide has real refractive index $n_{0,1} = n_{1,1} = n_{2,1} = 3.465$; note that the indices $n_{2,0}$ and $n_{2,1}$ only appear in the three-dimer case.

The two-dimer system can be described by the coupled mode equation,

$$-i\partial_z \begin{pmatrix} E_1(z) \\ E_2(z) \\ E_3(z) \\ E_4(z) \end{pmatrix} = \begin{pmatrix} \beta_R + i\beta_I & g_d & 0 & g_N \\ g_d & \beta_R & g_N & 0 \\ 0 & g_N & \beta_R + i\beta_I & g_d \\ g_N & 0 & g_d & \beta_R \end{pmatrix} \begin{pmatrix} E_1(z) \\ E_2(z) \\ E_3(z) \\ E_4(z) \end{pmatrix}, \quad (31)$$

where the imaginary part of the propagation constant, $\beta_I \approx 723.460$ m^{-1} , and the coupling parameters, g_d and g_N , are all recovered from COMSOL after some analysis. We analyze two configurations, a square one with separation distances $d_x = d_y = 2.790$ μm , where the intra- and inter-dimer couplings are equal, $g_d = g_N \approx 1701.467$ m^{-1} ; and a rectangular one, with $d_x = 2.790$ μm and $d_y = 3.906$ μm , with couplings $g_d \approx 1701.467$ m^{-1} and $g_N \approx 564.241$ m^{-1} . The common real part of the propagation constant, β_R , provides a common overall phase for all the field mode amplitudes, which is irrelevant for the analysis. We consider as input the superposition of two Gaussian beams, each a plane wavefront polarized in the vertical direction with waist radius $\omega_0 = 3.155$ μm , impinging at the lossy fiber of each dimer.

This array can be mapped to a necklace composed by two PT-symmetric dimers,

$$-i\partial_z \begin{pmatrix} \mathcal{E}_1(z) \\ \mathcal{E}_2(z) \\ \mathcal{E}_3(z) \\ \mathcal{E}_4(z) \end{pmatrix} = \begin{pmatrix} i\gamma & g_d & 0 & g_N \\ g_d & -i\gamma & g_N & 0 \\ 0 & g_N & i\gamma & g_d \\ g_N & 0 & g_d & -i\gamma \end{pmatrix} \begin{pmatrix} \mathcal{E}_1(z) \\ \mathcal{E}_2(z) \\ \mathcal{E}_3(z) \\ \mathcal{E}_4(z) \end{pmatrix}, \quad (32)$$

with the mapping function $E(z) = e^{i\beta_R z} e^{-\beta_I z} \mathcal{E}(z)$ that provides an approximated gain/loss given by the parameter $\gamma = \beta_I/2 \approx 362.730$ m^{-1} . In order to replicate the output of the effective dimer \hat{H}_0 , we use an in-phase superposition of the Gaussian beams, Fig. 3(b), and a π -dephased superposition, Fig. 3(c), to replicate the output of the effective dimer \hat{H}_1 . We retrieve from the simulation the values for the vertical component of the electric field at the propagation axis of each waveguide and use them to calculate the renormalized power within each fiber; that is, the power in the fiber divided by the power in the two fibers of its corresponding dimer,

$$P_{j,k}(z) = \frac{|E_y[d_x(-1)^{j+k}, d_y(-1)^j, z]|^2}{|E_y[d_x(-1)^j, d_y(-1)^j, z]|^2 + |E_y[d_x(-1)^{j+1}, d_y(-1)^j, z]|^2}. \quad (33)$$

In the homogeneous coupling configuration, addressing the first effective dimer provides oscillations of the renormalized power with approximated propagation constant $\Omega_0 \approx 3383.546$ m^{-1} as shown in Fig. 4(a). Addressing the second effective dimer produces propagation only through fibers ($j = 0, k = 0$) and ($j = 1, k = 0$), Fig. 4(b), as predicted by

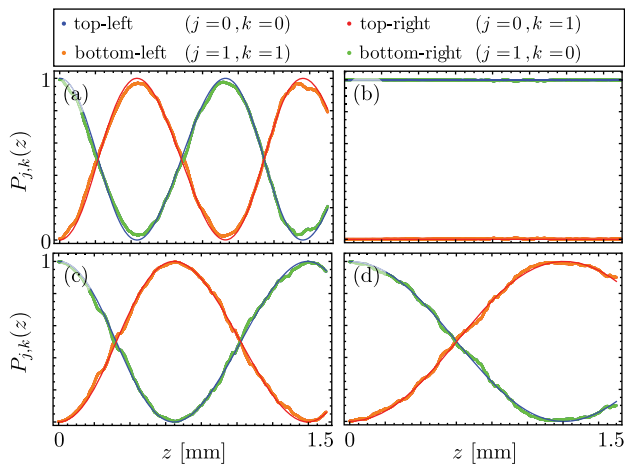


Fig. 4. Renormalized power propagation, $P_{j,k}(z)$, showing output replication for (a), (b) homogeneous and (c), (d) inhomogeneous couplings. The dots represent finite element propagation and the lines the analytic coupled mode approximation. See text for details.

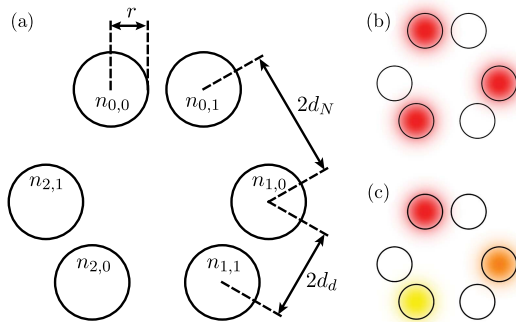


Fig. 5. (a) Waveguide geometry used in the finite element simulation and electric field input for replication of the (b) first and (c) second effective dimers. In (b) and (c), red corresponds to an in-phase beam, orange corresponds to a $(2\pi/3)$ -dephased beam, and yellow corresponds to a $(4\pi/3)$ -dephased one.

the coupled-mode equations. In the inhomogeneous coupling configuration, addressing the first and second effective dimers provides renormalized power oscillations with approximated propagation constants $\Omega_0 \approx 2250.632 \text{ m}^{-1}$, Fig. 4(c), and $\Omega_1 \approx 1243.131 \text{ m}^{-1}$, Fig. 4(d), in that order, as predicted by coupled mode theory.

For the sake of completeness, we also simulate a necklace of three dimers in the homogeneous and inhomogeneous configurations. The intra- and inter-dimer distances are the same as those used for the four-waveguide necklace. In the homogeneous configuration, these distances are $d_d = d_N = 2.790 \text{ }\mu\text{m}$, whereas in the inhomogeneous configuration their values are $d_d = 2.790 \text{ }\mu\text{m}$ and $d_N = 3.906 \text{ }\mu\text{m}$. These configurations are sketched in Fig. 5(a). For each configuration, we propagated an initial Gaussian beam superposition to address the first effective dimer ($j = 0$), Fig. 5(b), where the three beams are all in-phase, and the second effective dimer ($j = 1$), Fig. 5(c), where the second beam has a $2\pi/3$ dephasing and the third a $4\pi/3$ dephasing with respect to the first input beam.

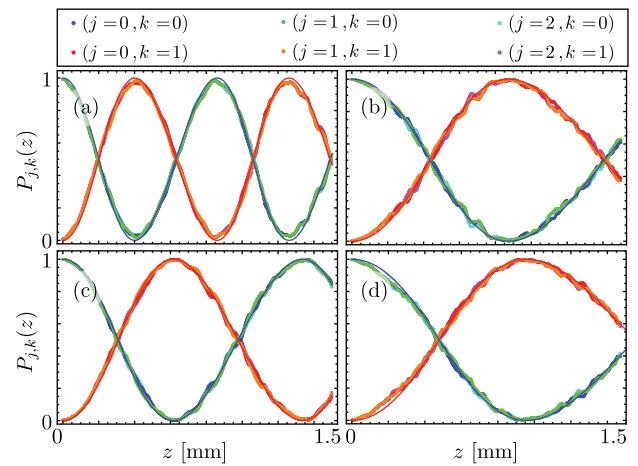


Fig. 6. Renormalized power propagation, $P_{j,k}(z)$, showing output replication for (a), (b) homogeneous and (c), (d) inhomogeneous couplings. The dots represent finite element propagation and the lines the analytic coupled mode approximation. See text for details.

In the homogeneous case, we find effective coupling values $g = g_d = g_N = 1836.114 \text{ m}^{-1}$ and an effective loss/gain parameter $\beta_I = 766.328 \text{ m}^{-1}$, leading to approximated propagation constants $\Omega_0 = 3652.173 \text{ m}^{-1}$ and $\Omega_1 = \Omega_2 = 1795.670 \text{ m}^{-1}$. On the other hand, for the inhomogeneous case the equivalent effective parameters found are $g_d = 1836.114 \text{ m}^{-1}$, $g_N = 666.727 \text{ m}^{-1}$, $\beta_I = 572.178 \text{ m}^{-1}$, and lead to approximated propagation constants $\Omega_0 = 2350.850 \text{ m}^{-1}$ and $\Omega_1 = \Omega_2 = 1457.138 \text{ m}^{-1}$ for the effective diagonal block dimers. Figure 6 shows the renormalized power propagating through our optical necklaces simulated by finite element methods (dots), as well as our analytic result (solid lines). Port replication through the homogeneous necklace addressing the first and second effective dimers is shown in Figs. 6(a) and 6(b), in that order. The equivalent for the inhomogeneous necklace is shown in Figs. 6(c) and 6(d). Note that the mode-coupling and finite element results are in good agreement for all propagation distances for both the homogeneous and inhomogeneous necklaces when the first, Figs. 6(a) and 6(c), and second, Figs. 6(b) and 6(d), effective dimers are addressed.

5. CONCLUSIONS

We have presented a group theoretical analysis for the mode-coupling description of light propagating through so-called necklaces of PT-symmetric dimers. We showed that the coupled mode matrix comprising the field dynamics in these arrays can be written as a composition of elements of the cyclic group and the $(2 + 1)$ -dimensional Lorentz group. Using the fact that the cyclic subcomponent is straightforward to diagonalize, we demonstrated that the necklace effective dynamics is provided by N uncoupled PT-symmetric dimers, where N is the number of dimer copies in the necklace. For an even number of copies and homogeneous distribution of the waveguides, there is always at least one effective dimer in the broken symmetry phase. The PT symmetry of these necklaces can be

restored by making the inter- and intra-dimer couplings different in value. In general, for necklaces with three or more dimer copies, there will always be pairs of effective dimers that are the complex conjugated of each other and will show identical light power propagation.

We compared our effective mode-coupling analysis with finite element simulations to obtain good agreement in all cases studied. Our analytic results and computational simulations show that it is possible to use impinging light to switch between the different effective dynamics provided by a necklace of PT-symmetric dimers and replicate their outputs all over the necklace. Furthermore, our results demonstrate that it is plausible to design devices where oscillations in the PT-symmetric regime can be switched to linear and exponential field amplitude dynamics at the Kato exceptional point and in the broken-symmetry regime, respectively, by changing the relative phases of input fields. While our results were simulated using experimental parameters from laser inscribed waveguides, they are valid for multicore fibers, toroidal cavities, and electronic devices as well.

As a final note, we want to emphasize that port replication is an intrinsic characteristic of the underlying cyclic symmetry. Thus, we could replace the PT-symmetric dimer with a different dimer and we could replicate the effective dynamics provided by the new symmetry.

Funding. Consejo Nacional de Ciencia y Tecnología (CONACYT) (Catedra Grupal #551, FORDECYT #290259); Red de Tecnologías Cuánticas.

Acknowledgment. D. J. Nodal Stevens acknowledges financial support from Red de Tecnologías Cuánticas through the program Verano de Investigación Científica and the Photonics and Mathematical Optics group hospitality. B. M. Rodríguez-Lara acknowledges support from the Photonics and Mathematical Optics Group at Tecnológico de Monterrey and Consorcio en Óptica Aplicada through CONACYT FORDECYT #290259 project grant.

REFERENCES

1. S. Somekh, E. Garmire, A. Yariv, H. L. Garvin, and R. G. Hunsperger, "Channel optical waveguide directional couplers," *Appl. Phys. Lett.* **22**, 46–47 (1973).
2. Y. Chen, A. W. Snyder, and D. N. Payne, "Twin core nonlinear couplers with gain and loss," *IEEE J. Quantum Electron.* **28**, 239–245 (1992).
3. C. M. Bender, "Real spectra in non-Hermitian Hamiltonians having PT-symmetry," *Phys. Rev. Lett.* **80**, 5243–5246 (1998).
4. C. M. Bender, "Introduction to PT-symmetric quantum theory," *Contemp. Phys.* **46**, 277–292 (2005).
5. A. Ruschhaupt, F. Delgado, and J. G. Muga, "Physical realization of PT-symmetric potential scattering in a planar slab waveguide," *J. Phys. A* **38**, L171–L176 (2005).
6. R. El-Ganainy, K. G. Makris, D. N. Christodoulides, and Z. H. Musslimani, "Theory of coupled optical PT-symmetric structures," *Opt. Lett.* **32**, 2632–2634 (2007).
7. J. D. Huerta Morales, J. Guerrero, S. Lopez-Aguayo, and B. M. Rodríguez-Lara, "Revisiting the optical PT-symmetric dimer," arXiv: 1607.02782 (2016).
8. R. El-Ganainy, K. G. Makris, M. Khajavikhan, Z. D. Musslimani, S. Rotter, and D. N. Christodoulides, "Non-Hermitian physics and PT symmetry," *Nat. Phys.* **14**, 11–19 (2018).
9. A. Guo, G. J. Salamo, D. Duchesne, R. Morandotti, M. Volatier-Ravat, V. Aimez, G. A. Siviloglou, and D. N. Christodoulides, "Observation of PT-symmetric breaking in complex optical potentials," *Phys. Rev. Lett.* **103**, 093902 (2009).
10. C. E. Rüter, K. G. Makris, R. El-Ganainy, D. N. Christodoulides, and D. Kip, "Observation of parity-time symmetry in optics," *Nat. Phys.* **6**, 192–195 (2010).
11. M. Ornigotti and A. Szameit, "Quasi PT-symmetry in passive photonic lattices," *J. Opt.* **16**, 065501 (2014).
12. B. Peng, S. Ozdemir, F. Lei, F. Monifi, M. Gianfreda, G. Long, S. Fan, F. Nori, C. Bender, and L. Yang, "Parity-time-symmetric whispering-gallery microcavities," *Nat. Phys.* **10**, 394–398 (2014).
13. H. Hodaei, M.-A. Miri, M. Heinrich, D. N. Christodoulides, and M. Khajavikhan, "Parity-time symmetric microring lasers," *Science* **346**, 975–978 (2014).
14. B. M. Rodríguez-Lara and J. Guerrero, "Optical finite representation of the Lorentz group," *Opt. Lett.* **40**, 5682–5685 (2015).
15. I. V. Barashenkov, L. Baker, and N. V. Alexeeva, "PT-symmetry breaking in a necklace of coupled optical waveguides," *Phys. Rev. A* **87**, 033819 (2013).
16. K. Li and P. G. Kevrekidis, "PT-symmetric oligomers: analytical solutions, linear stability, and nonlinear dynamics," *Phys. Rev. E* **83**, 066608 (2011).
17. D. A. Zezyulin and V. V. Konotop, "Nonlinear modes in finite-dimensional PT-symmetric systems," *Phys. Rev. Lett.* **108**, 213906 (2012).
18. K. Li, P. G. Kevrekidis, B. A. Malomed, and U. Günther, "Nonlinear PT-symmetric plaquettes," *J. Phys. A* **45**, 444021 (2012).
19. Z. Liu, Q. Zhang, X. Liu, Y. Yao, and J.-J. Xiao, "Absence of exceptional points in square waveguide arrays with apparently balanced gain and loss," *Sci. Rep.* **6**, 22711 (2016).
20. S. Longhi, "PT phase control in circular multi-core fibers," *Opt. Lett.* **41**, 1897–1900 (2016).
21. B. M. Rodríguez-Lara, R. El-Ganainy, and J. Guerrero, "Symmetry in optics and photonics: a group theory approach," *Sci. Bull.* **63**, 244–251 (2018).
22. J. J. Sylvester, "LX. Thoughts on inverse orthogonal matrices, simultaneous sign successions, and tessellated pavements in two or more colours, with applications to Newton's rule, ornamental tile-work, and the theory of numbers," *Philos. Mag.* **34**, 461–475 (1867).
23. N. V. Alexeeva, I. V. Barashenkov, and Y. S. Kivshar, "Solitons in PT-symmetric ladders of optical waveguides," *New J. Phys.* **19**, 113032 (2017).
24. J. D. Huerta Morales and B. M. Rodríguez-Lara, "Photon propagation through linearly active dimers," *Appl. Sci.* **7**, 587 (2017).
25. T. Kato, *Perturbation Theory for Linear Operators* (Springer-Verlag, 1995).
26. A. H. Nejadmalayeri, P. R. Herman, J. Burghoff, M. Will, S. Nolte, and A. Tünnermann, "Inscription of optical waveguides in crystalline silicon by mid-infrared femtosecond laser pulses," *Opt. Lett.* **30**, 964–966 (2005).
27. M. Chambonneau, Q. Li, M. Chanal, N. Sanner, and D. Grojo, "Writing waveguides inside monolithic crystalline silicon with nanosecond laser pulses," *Opt. Lett.* **41**, 4875–4878 (2016).